CHARACTERIZATION OF LUNAR REGOLITH VIA PASSIVE REMOTE SENSING IN MICROWAVE SPECTRUM FROM 1 TO 10 GHZ. M. Aksoy[1], I. Walter[1], D. M. Hollibaugh Baker[2], J. R. Piepmeier[2], [1]University at Albany, State University of New York, 1400 Washington Ave, Albany, NY 12222, USA, maksoy@albany.edu, [2]NASA Goddard Space Flight Center, 8800 Greenbelt Rd, Greenbelt, MD 20771, USA, david.m.hollibaugh-baker@nasa.gov.

Introduction: In this study, through a set of microwave radiation simulations, we have demonstrated that microwave radiometer measurements of lunar regolith at multiple frequencies from 1 to 10 GHz can be used to infer important regolith characteristics such as regolith thickness, internal temperature and density profiles, and chemical composition.

Theoretical Background: This study has been performed with following considerations regarding physical, thermal and electrical properties of lunar regolith, and electromagnetic radiation from regolith surface:

Regolith Stratigraphy: The lunar regolith is formed of different fragmented materials and it can be modeled as a layered medium where each layer may have different physical, chemical, and thermal properties.

Regolith Density: Bulk density of lunar regolith, ρ is assumed to follow the expression described in [1] versus depth, z:

$$\rho(z) = \rho_d - (\rho_d - \rho_s)e^{-z/H} \quad (1)$$

where ρ_s is the surface density, H is the densification parameter, and ρ_d is the density at depths $z \gg H$. ρ_s and ρ_d are assumed to be 1.30 and 1.92 g/cm^3, respectively based on the Apollo measurements [2]. Fig. 1 plots $\rho(z)$ for two different H values (H = 10 and 100 cm).

Regolith Temperature: Physical temperature, T, in lunar regolith versus depth, z, and time, t, is described by the solution of the following one-dimensional heat conduction equation (neglecting advection):

$$\rho(z)c(z,T)\frac{\partial T}{\partial t} = \frac{\partial}{\partial z}\left(k(z,T)\frac{\partial T}{\partial z}\right) + Q(z,T) \quad (2)$$

where $\rho(z)$, $c(z,T)$, $k(z,T)$, and $Q(z,T)$ are bulk density (g/cm^3), specific heat (Jg^{-1}K^{-1}), thermal conductivity (Js^{-1}K^{-1}cm^{-1}), and internal heat flux (Js^{-1}cm^{-2}), respectively. A numerical solution process for this equations is given in [3]. Fig. 1 also depicts regolith temperature profiles during lunar night based on equation (2) for two constant internal flux values (Q = 0 and 2×10^{-6} Js^{-1}cm^{-2}).

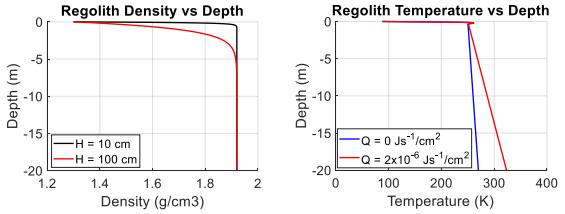

Fig. 1. Regolith density and temperature profiles versus depth for two densification and internal flux values.

Regolith Complex Permittivity: It is accepted that the real part of the relative permittivity (ϵ') of lunar regolith has the following power law relation with the bulk regolith density [4]:

$$\epsilon'(z) \approx 10^{0.27\rho(z)} \quad (3)$$

On the other hand, the imaginary part of the relative permittivity (ϵ'') is expressed as a function of regolith density and chemical composition, p_{ch}(percentage of TiO_2+FeO amount), based on Apollo measurements and previous analyses with Chang'E-1 and 2 radiometer data [1,5]:

$$\epsilon''(z) \approx \epsilon'(z) \times 10^{0.038p_{ch}+0.312\rho(z)-3.260} \quad (4)$$

Electromagnetic Emission Model: Using the complex permittivity of lunar regolith, the electromagnetic attenuation coefficient can be computed for a specific depth, z, and frequency, f, as [6]:

$$\alpha(f,z) = -2 \times imag\left\{2\pi f\sqrt{\mu_o\epsilon_o\left(\epsilon'(z) - i\epsilon''(z)\right)}\right\} \quad (5)$$

Then, assuming the electromagnetic scattering and internal reflections are negligible within the regolith, normal incidence brightness temperatures at the regolith surface, $T_B(z=0,f)$ can be calculated as a function of frequency as:

$$T_B(z=0,f) = \int_{z_{deep}}^{z=0}\left[\prod_{z'=z}^{z'=0}\Gamma(f,z')\right]\alpha(f,z)\,T(z)e^{-\int_{z'=z}^{z'=0}\alpha(f,z)\,dz'}dz \quad (6)$$

where $\Gamma(f,z')$ and $T(z)$ are the amplitude squared of the Fresnel transmission coefficient between regolith layers at depth z' for frequency f and the physical regolith temperature at depth z, respectively.

Simulations and Results: Normal incidence surface brightness temperatures have been calculated at frequencies from 1 to 10 GHz for regolith thickness values between 5 and 20 meters as shown in Fig. 2(a). The density and temperature profiles are assumed to be what is shown in Fig. 1 with H= 10 cm and Q= 0 Js^{-1}cm^{-2}, respectively; p_{ch} is taken as 10%, and the bedrock is accepted to be at the same temperature as the deepest regolith layer with complex permittivity of $5.87 + 0.0086i$, a value measured at the Apollo 15 site [7].

It can be seen that, since electromagnetic penetration depth decreases with frequency, only brightness temperatures at lower frequencies are sensitive to changes

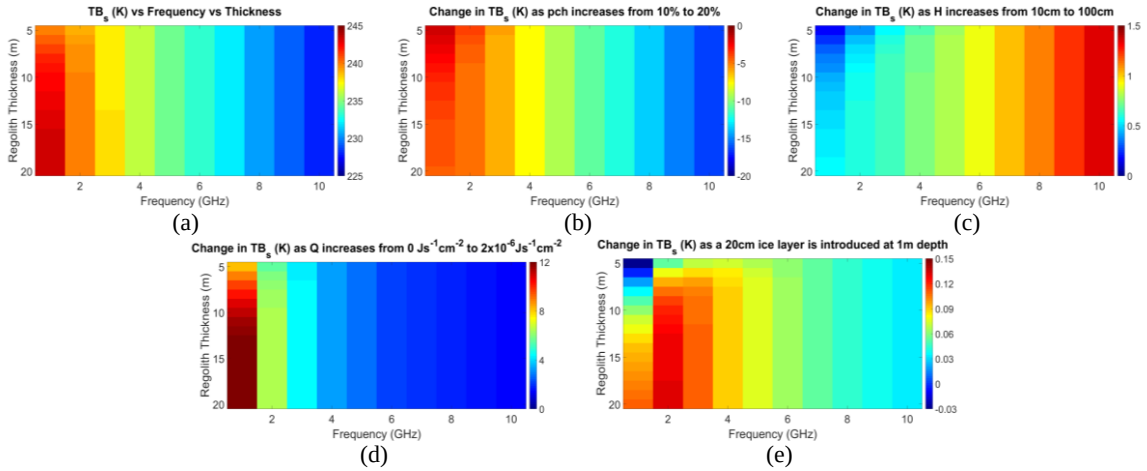

Fig. 2. (a) Regolith surface brightness temperatures at frequencies from 1 to 10 GHz for regolith thickness values between 5 and 20 meters, and changes in regolith surface brightness temperatures as (b) p_{ch} varies from 10% to 20%, (c) H varies from 10 cm to 100 cm, (d) Q varies from 0 to 2×10^{-6} $Js^{-1}cm^{-2}$, and (e) a 20 cm thick ice layer is introduced at 1 meter depth.

in regolith thickness. For instance, brightness temperatures at 1 GHz increases with thickness until 20 meters, whereas no significant change is observed at frequencies above 4 GHz as only top layers contribute to surface emissions at these frequencies. Thus, changes in brightness temperatures only at lower frequencies may imply changes in regolith thickness.

Fig. 2(b) demonstrates differences in surface brightness temperatures as p_{ch} is increased from 10% to 20%. Increased p_{ch} leads to higher attenuation, thus shorter penetration depths. Therefore, brightness temperatures in general decrease to reflect cooler regolith closer to the surface. The decrease is more severe at higher frequencies, e.g., >15 K at 10 GHz vs <5 K at 1 GHz, as these frequencies are sensitive to layers near the surface where the temperature gradient is large. Thus, changes in brightness temperatures mainly at high frequencies may imply changes in chemical composition in the regolith.

Increase in H, on the other hand, results in less dense regolith and reduced attenuation; thus, brightness temperatures increase. Again, its impact, as seen from Fig. 2(c) , is more substantial at higher frequencies since the physical temperature gradient is larger in top layers.

Higher internal flux values increase the temperature rise with depth in deep regolith. Thus, larger Q values increase the surface brightness temperature, as shown in Fig. 2(d), mainly at low frequencies where deep regolith has a considerable contribution to the surface emissions. At large frequencies, e.g., >8 GHz, the impact is minimal.

Moreover, microwave radiometer measurements within the 1-10 GHz spectrum can be sensitive to ice layers buried in the regolith. Fig. 2(e) demonstrates the changes in surface brightness temperatures when a 20-cm thick ice layer (with the same temperature as regolith) is introduced at 1 meter depth in regolith. The ice is more transparent then regolith at these frequencies; thus, the ice layer reduces attenuation and influences the surface brightness temperatures mostly at frequencies sensitive to that specific depth. For 1 meter, as shown in Fig. 2(e), this frequency is ~2 GHz. The depth of the ice layer and its thickness determines the amount of change in surface brightness temperatures and the most sensitive frequency to such changes. For instance, the impacts of ice layers closer to the surface will be more notable at higher frequencies.

Finally, it is important to recognize that the impacts of thermal, physical and chemical properties on the surface brightness temperatures shown here can be coupled rather than independent; thus, auxiliary information from other types of lunar measurements may be necessary to constrain retrieval studies for regolith characterization.

Acknowledgments: This research has been funded and supported by the National Aeronautics and Space Administration's (NASA) Lunar Data Analysis Program (Grant # 80NSSC20K0312).

References: [1] Vasavada, A. R. et al. (2012) *JGR: Planets*, *117*, E12. [2] French, B. M. et al. (1991) *Lunar sourcebook: A user's guide to the Moon*, CUP Archive. [3] Hayne, P. O. et al. (2017) *JGR: Planets*, *122.12*, 2371-2400. [4] Montopoli, M. et al. (2011) *Radio Science*, *46.01*, 1-13. [5] Liu, C. and Chen P. (2016) *IGARSS*, 2688-2691. [6] Pozar, D. M. (2009) *Microwave engineering*, John Wiley & Sons. [7] Nakamura, Y. et al. (1975) *The Moon*, *13.1-3*, 57-66.